NIH Public Access
Author Manuscript
J Cardiovasc Electrophysiol. Author manuscript; available in PMC 2009 November 5.

Published in final edited form as:
J Cardiovasc Electrophysiol. 2008 October ; 19(10): 1080–1089. doi:10.1111/j.1540-8167.2008.01201.x.

Spatial Distribution and Extent of Electroporation by Strong Internal Shock in Intact Structurally Normal and Chronically Infarcted Rabbit Hearts

SEOK C. KIM, M.S.[*,†], **AMIT VASANJI, Ph.D.**[‡], **IGOR R. EFIMOV, Ph.D.**[†,§], and **YUANNA CHENG, M.D., Ph.D.**[*,†]

[*] Department of Molecular Cardiology, Cleveland Clinic, Cleveland, Ohio, USA

[‡] Department of Biomedical Engineering, Cleveland Clinic, Cleveland, Ohio, USA

[†] Department of Biomedical Engineering, Case Western Reserve University, Cleveland, Ohio, USA

[§] Department of Biomedical Engineering, Washington University, St. Louis, Missouri, USA

Abstract

Introduction—Although life-saving, a strong internal defibrillation shock may temporarily or permanently damage the heart via disruption of cell membranes (electroporation). Spatial extent of electroporation in intact, normal, or infarcted hearts has not been investigated. In this study, shock-induced electroporation in intact rabbit hearts with and without chronic (>4 weeks) left ventricular myocardial infarction (MI) was characterized.

Methods and Results—A coil shock electrode was inserted in the right ventricle of Langendorff-perfused hearts. One truncated exponential monophasic shock (+300 V, 8 ms) was delivered by a 150 μF capacitor clinical defibrillator while the heart was perfused with membrane-impermeant dye propidium iodide (PI). The heart was sectioned transversely, and uptake of PI into ventricular myocardium through electropores was quantified. Histological evaluation was performed via Masson's trichrome staining. PI accumulation was minimal in the control (n = 3) and MI (n = 3) hearts without shock. Following shock delivery, (1) in control (n = 5) and MI (n = 5) hearts, electroporation mostly occurred near the shock electrode and was longitudinally distributed along the active region of the shock electrode; (2) in MI group, electroporation was significantly increased ($P < 0.05$) in the surviving anterior epicardial layers of the infarcted region; and (3) between the control and MI groups, the overall extent of electroporation was similar.

Conclusion—Shock-induced electroporation was spatially dependent on the location and dimension of the active region of the shock electrode. The overall extent of electroporation in the MI heart was comparable with the control heart, but the surviving anterior epicardial layers in the infarcted region were more susceptible to electroporation.

Keywords

electroporation; defibrillation; myocardial infarction; propidium iodide

Address for correspondence: Yuanna Cheng, M.D., Ph.D., Department of Molecular Cardiology, NE61, Cleveland Clinic, 9500 Euclid Avenue, Cleveland, OH 44195, USA. Fax: 216-445-4166; chengy@ccf.org.

NIH-PA Author Manuscript
NIH-PA Author Manuscript
NIH-PA Author Manuscript

NIH-PA Author Manuscript

NIH-PA Author Manuscript

NIH-PA Author Manuscript

Introduction

Application of a defibrillation shock to the heart is the most effective and immediate therapy against lethal ventricular arrhythmia. While the defibrillation shock can rescue patients from life-threatening arrhythmias, the shock may have unfavorable ramifications due to its excitatory and suppressive effects.[1–5] A strong electrical shock may also temporarily or permanently damage the heart via formation of aqueous pores referred to as electropores due to disruption of the cell membrane (electroporation).

Experimentally, electroporation is commonly used to provide access for transport of DNA, RNA, or other macro-molecules into the intracellular space, and has been extensively studied.[6–9] The effects of electroporation on cardiac electrical activity have been investigated in isolated myocyte,[10–12] cultured myocyte,[13] and cardiac tissue[14–16] preparations. During measurements of the transmembrane potential change, elevated diastolic potential,[13,14,17,18] upwardly shifted or depolarized resting membrane potential, decreased action potential amplitude, and reduced rate of rise during the upstroke of action potential[3,19] have been attributed to the occurrence of electroporation. Electroporation has also been incorporated into computer models of postshock transmembrane potential change in order to provide a better fit between empirical data and simulations, as well as to explain its role in defibrillation.[20–23]

Electroporation affects the cellular responses to an electrical shock and, therefore, may play a crucial role in determining the overall response of the heart to a defibrillation shock. Although studies have been performed to evaluate the impact of electroporation on cardiac electrical activities as well as the effect of shock-induced transmembrane polarization pattern on defibrillation via the virtual electrode polarization hypothesis,[24–26] the role of electroporation in defibrillation remains ambiguous.[3,18,22,23,27] More fundamentally, a question regarding the spatial distribution and extent of electroporation by a defibrillation shock in the intact heart has not been addressed.

Clinically, patients with a prior history of left ventricular (LV) myocardial infarction (MI) have an increased risk of lethal arrhythmia.[28–30] An implantable cardioverter defibrillator (ICD) lead is commonly implanted in the right ventricle (RV) of these patients to deliver rescue shocks that can terminate otherwise lethal arrhythmias. The spatial vulnerability of the MI heart to shock-induced electroporation, however, has never been studied.

To address this issue, we have assessed the spatial distribution and extent of shock-induced electroporation in intact, structurally normal rabbit hearts and rabbit hearts with healed myocardial infarction (more than 4 weeks post-MI). A membrane-impermeant dye, propidium iodide (PI) was used to characterize electroporation.[6,13,19,31] The spatial characterization of electroporation may be further used to advance targeted transportation of genes or drugs into the intracellular space[6,32] and ablation therapy by electroporation.[33] Evaluation of the spatial distribution and extent of shock-induced electroporation may contribute to an improved understanding of the mechanisms of defibrillation, with respect to the occurrence and impact of electroporation. Spatial comparison of electroporation between the normal and MI hearts may aid identification of the pro- and antiarrhythmogenic aspects of electroporation, and facilitate development of safer and more effective defibrillation therapies.

Methods

The animal research protocol was approved by the Institutional Animal Care and Use Committee of the Cleveland Clinic. Animals included in this study were housed in the animal facility under veterinary supervision and received humane care as set forth in *Guide for the Care and Use of Laboratory Animals* published by the National Institutes of Health (NIH Publication No. 85-23, revised 1996).

NIH-PA Author Manuscript

NIH-PA Author Manuscript

NIH-PA Author Manuscript

Animal Model

Sixteen adult New Zealand White rabbits of either sex weighing 3 to 4 kg (Harlan, Indianapolis, IN, USA) were used in this study. Eight rabbits were used as controls in which no surgical infarction procedure was performed. A chronic MI was created in eight rabbits, as described in detail previously.[4,34] Briefly, the rabbits were anesthetized and intubated for the left thoracotomy. A long-lasting antibiotic was administered preoperatively. The heart rate, ECG, and oxygen and carbon dioxide saturation levels were continuously monitored. Depending on the branching pattern,[35,36] the lateral or posterolateral division of the left coronary artery was identified. To minimize occurrence of ventricular arrhythmias, 1 mg/kg lidocaine was intravenously injected immediately before the ligature placement. The target artery was ligated approximately at a level of 40% from the apex. A chest tube was inserted, and the chest was closed by approximating the ribs on both sides of the incision. The chest was sealed by four suture layers, and the chest tube was withdrawn while negative pressure was applied. Postoperatively, an analgesic was given immediately following the surgery and twice a day thereafter for an additional two days. Following infarction, the rabbits were allowed to heal at least for 4 weeks.

Heart Preparation

The acute heart preparation and experimental setup have also been described in detail.[4,37,38] Briefly, the intact control or MI heart was isolated and placed on the cannula of a modified Langendorff apparatus for in vitro retrograde perfusion via the aorta. Temperature- and pH-controlled, modified oxygenated Tyrode solution was filtered through 2 μm Millipore filters before perfusion through the heart. A custom-modified 10 mm coil (1.8 mm in diameter) defibrillation electrode was inserted into the RV cavity through the pulmonary artery. The distal tip was consistently positioned against the anterior RV free wall and the septum at the very apex (Fig. 2C). The shock electrode was composed of a 6 mm nonconducting inactive region and a 10 mm active region. The 50 mm coil reference electrode was placed in a U-shape with the arms pointing upward while completely immersed in the perfusion bath. The reference electrode was parallel to the posterior epicardial surface of the heart, positioned approximately 10–20 mm behind and above the tip of the apex. The reference electrode (RE) position is schematically illustrated in Figure 1A. A bipolar pacing electrode was placed at the apex of the posterior RV to pace the heart at a basic cycle length of 300 ms.

Experimental Protocol

The heart was suspended and equilibrated in the Tyrode solution-filled perfusion chamber for 30–40 minutes. As previously described,[25] the anterior surface of the heart including both LV and RV was in slight contact with the flat glass wall of the perfusion chamber in order to simulate high impedance interface between the anterior heart muscle and elements of thorax such as fat and sternum bones in vivo. Fifteen minutes prior to shock delivery, the perfusate was changed to a Tyrode solution containing 30 μM PI (Sigma-Aldrich, St. Louis, MO, USA). In five control and five MI hearts, one +300-V, 8 ms truncated exponential monophasic shock was delivered by a 150 μF capacitor defibrillator (HVS-02; Ventritex, Sunnyvale, CA, USA) during the repolarization phase, approximately 100 ms following the QRS complex. A shock of high intensity (300 V) was used to ensure the occurrence of electroporation in this model. The anodal polarity was chosen because it is less likely to induce postshock arrhythmia compared with the cathodal monophasic shock. No postshock arrhythmia was induced in this study. Mean delivered energy and impedance recorded by the defibrillator were 5.8 ± 0.1 J and 43 ± 2 Ω in the control group (n = 5) and 5.7 ± 0.0 J (P = 0.14 vs control) and 46 ± 1 Ω (P < 0.05) in the MI group (n = 5). No shock was delivered in three control and three MI hearts. Postshock perfusion with 30 μM PI-containing Tyrode solution was continued for 15 minutes. During the 40-minute washout, the heart was perfused with Tyrode solution without PI. The

NIH-PA Author Manuscript

NIH-PA Author Manuscript

NIH-PA Author Manuscript

heart was removed from the perfusion chamber and placed in ice-cold Tyrode solution to reduce cardiac contraction. The atria were excised, exposing the intact ventricles and the septum. The heart was embedded in cooled Tissue-Tek Embedding Medium (OCT; Sakura Finetek, Torrance, CA, USA), frozen in cold isopentane (2-Methylbutane; Sigma-Aldrich), and stored at −80°C. 20-μm thick transverse sections were cut at −20°C in 800 μm intervals from the apex toward the base, mounted onto Superfrost Plus microslides (75×25 mm; VWR, West Chester, PA, USA) or custom-ordered Superfrost Plus large slides (75×38 mm; Fisher Scientific, Pittsburgh, PA, USA), and stored at −20°C.

Fluorescence Study

The apex-to-base lengths of the ventricles from which samples were collected were 18.26 ± 1.71 mm in the control group (n = 8) and 18.53 ± 1.91 mm in the MI group (n = 8, P = 0.77). Eleven ± 3 slides were visually selected from the full range of transverse sections according to the PI fluorescence distribution pattern. PI fluorescence was imaged using a digital camera (RTE/CCD-1300 Y/HS; Roper Scientific, Trenton, NJ, USA) on an epifluorescence microscope (DMRXA; Leica Microsystems, Wetzlar, Germany) with a Texas Red filter (5× objective). The camera exposure was kept constant within the same heart to minimize variations due to imaging condition. A motorized stage (H138 ProScan; Prior Scientific, Rockland, MA, USA) and MetaMorph 6.21r1 (Molecular Devices, Sunnyvale, CA, USA) software generated a mosaic image of the entire cross section with 4 μm/pixel resolution. A representative transverse section from the control heart stained with PI upon shock delivery is shown in Figure 1. The entire ventricular myocardium was visualized and analyzed based on its autofluorescence at exposure times in which localized PI-stained nuclei appeared brightly. Since segmented PI fluorescence only represented areas of nuclear staining (Fig. 1A), electroporated tissue area was quantified as the area of autofluorescent tissue within the boundaries of PI accumulation. Representative tissue traced for positive PI staining is shown in Figure 1B. PI cluster boundary tracing and tissue area quantification were performed in an automated fashion using Image-Pro 6.2 (Media Cybernetics, Bethesda, MD, USA). The total tissue volume was obtained via linear piecewise integration of myocardial cross-sectional areas along the long axis. Electroporated tissue volume was similarly integrated and quantified within the PI-cluster boundaries. The extent of electroporation was defined as electroporated tissue volume normalized to the total tissue volume (%PI Volume).

In analyzing the spatial extent of electroporation transversely with respect to the shock electrode position, the ventricles at each cutting plane was first divided into four regions (Fig. 1B). The first region encompassed the anterior and anterolateral RV free wall and approximately one-fourth of the septum (aRV) that was in a close vicinity to the shock electrode (SE). The three remaining regions were similarly categorized to include the posterior and posterolateral RV free wall and the adjacent septum (pRV), the anterior and anterolateral LV free wall and the adjacent septum (aLV), and the posterior and posterolateral LV free wall and the adjacent septum (pLV). In each of four regions except for the aRV region, three subregions were identified. The epicardial layer (Epi) was defined as a portion of the free wall from the epicardium to the mid-wall. The remaining free wall inclusive of the endocardium was considered as the endocardial layer (Endo). The septal region (Sep) included a portion of the septum within each respective region. In Figure 1B, the PI accumulations identified in Epi and Endo of the aLV region and in Sep of the pLV region are shown. The ventricular cross sections were divided into relatively simplified regions in order to reflect physiologically distinctive structures. During shock delivery, the extent of PI accumulation in the aRV region was large due to its close proximity to the shock electrode. No subdistinction was made in this region, and it was collectively considered as the shock electrode region. PI-stained tissue volumes in all four regions of the transverse sections were summed over the entire ventricles to yield the overall electroporated tissue volume.

NIH-PA Author Manuscript

NIH-PA Author Manuscript

NIH-PA Author Manuscript

Histology

The transverse sections used in the fluorescence study were stained using Masson's trichrome (American MasterTech, Lodi, CA, USA) for correlation of PI staining with structural changes. Histology images were captured by Retiga-SRV Fast 1394 camera (Q-Imaging, Surrey, British Columbia, Canada) on Leica DM5000B microscope (5× objective) with 1.28 μm/pixel resolution. A motorized stage (H101 ProScan, Prior Scientific) controlled via Turboscan software (Objective Imaging, Kansasville, WI, USA) running in Image-Pro enabled mosaic imaging of the entire cross section (Fig. 2A). Muscle (red) and fibrous MI scar tissue (blue) areas were quantified in an automated fashion using Image-Pro. Infarct size was expressed as a percentage of the fibrous tissue volume with respect to the whole left and right ventricular tissue volume (Fig. 2B).

Statistical Analysis

Summary group data are reported as mean ± SD. Statistical comparisons between two groups were performed using two-tailed, unpaired Student's *t*-tests. Differences were considered significant when $P < 0.05$.

Results

Myocardial Infarction in the Ventricles

Masson's trichrome staining confirmed the location and extent of MI in the ventricles, as shown in Figure 2. Control hearts (top panel, Fig. 2A) were mostly stained in red for muscle tissue. In the MI heart (bottom panel, Fig. 2A), loss of myocardium led to thinning of the free wall and fibrous scar tissue formation[39] (blue). The MI was always mostly transmural in the LV free wall and mainly confined in the anterior LV free wall, extending toward the lateral and posterior LV free wall. All MI hearts had characteristically similar pathologic features. In the infarcted free walls of all eight MI hearts, surviving endocardial and epicardial layers were observed. The endocardial layer was always found as a relatively thick layer, lining the endocardium. In the epicardium, a thin layer or islands of surviving cells were infiltrated by fibrous scar tissue. Figure 2B shows spatial quantification of the fibrous tissue content along the long axis of the heart. The fibrous infarct scar was mainly in the apical region. The infarct volume was 14.4 ± 4.9% (n = 8) of the whole ventricles. An MI heart preparation in the perfusion chamber is shown in Figure 2C.

Spatial Characterization of Electroporation in the Structurally Normal Hearts

First, the spatial distribution and extent of electroporation were characterized in control hearts (Fig. 3). In the control group without shock (n = 3), there was minimal PI accumulation (top panel, Fig. 3A). This minimal PI accumulation was sometimes found as randomly distributed, miniature speckles in transverse sections as illustrated in Figure 1B. When a shock (+300-V, 8 ms monophasic) was delivered, electroporation was evident, especially in the shock electrode (SE) region (bottom panel, Fig. 3A). The shock electrode and reference electrode (RE) positions are illustratively indicated in one fluorescence image. The histology images of the same transverse sections are shown in the top panel of Figure 2A. The whole ventricles are three-dimensionally (3D) reconstructed from these series of fluorescence (PI pseudocolored in red) and histology (muscle in green and fibrous tissue in blue) images (Movie 1; online supplement). In the interactive movie, the 3D ventricles can be freely oriented or zoomed in and out using the mouse cursor. In control hearts with shock, the extent of electroporation in the shock electrode region (gray traces, Fig. 3B) was closely related to the location and dimension of the active region of the shock electrode along the long axis. At the very apex near the inactive region of the shock electrode, there was virtually no PI accumulation. Within the range spatially corresponding to the location of the active region, approximately 6 to 16 mm

NIH-PA Author Manuscript

NIH-PA Author Manuscript

NIH-PA Author Manuscript

from the apex, electroporation was maximal. This electroporation distribution pattern was consistent and similar among all five hearts (individual traces, Fig. 3B). Total tissue area represents ventricular tissue area in the transverse sections (black traces). The circle markers indicate measurements made from the transverse sections shown in the bottom panel of Figure 3A. In all five control hearts with shock, electroporation always reached a transmural level in the anterior RV free wall (wall thickness: 2.2 ± 0.3 mm). In the septum, PI staining was transseptal in two hearts. The average depth of PI staining in five hearts was 60.9 ± 35.9% of the septum thickness (6.0 ± 2.6 mm).

The regional and overall extents of electroporation are summarized in Figure 3C and in Table 1. When no shock was delivered in the control hearts (striped gray), there was virtually no PI accumulation. In control hearts with shock (solid gray), the extent of electroporation was most apparent ($P < 0.05$) in the shock electrode region (SE) compared to the control hearts without shock. Within the control group with shock, the shock electrode region was significantly more electroporated than all remaining regions ($P < 0.05$). In the pRV, aLV, and pLV regions, there were only minute PI-positive traces. The overall normalized PI-positive tissue volume was increased ($P < 0.05$) to 5.9 ± 1.1% in the control group compared to the control hearts without shock.

Spatial Characterization of Electroporation in the Chronically Infarcted Hearts

The spatial distribution and extent of electroporation was similarly characterized in MI hearts (Fig. 4). As in the control group without shock, there was little PI accumulation in the MI hearts (top panel, Fig. 4A) when no shock was delivered (n = 3). Shock-induced electroporation was apparent in the MI group with shock (bottom panel, Fig. 4A) similarly to the control group with shock. However, PI-staining of the aLV Epi was different from the control group with shock (bottom panel, Fig. 3A) and from the MI group without shock (top panel, Fig. 4A). The same series of transverse sections are also shown in the bottom panel of Figure 2A for histological correlation. The interactive movie of this MI heart is provided as a supplement (Movie 2). The characteristic dependence of electroporation parallel to the shock electrode was similar to the control hearts with shock (Fig. 4B) as well as its consistency (individual traces, Fig. 4B). In all five MI hearts with shock, the PI staining was also transmural in the anterior RV free wall (wall thickness: 2.6 ± 0.3 mm). In the septum (septum thickness: 6.4 ± 0.7 mm), the average depth of electroporation in five hearts was 67.0 ± 30.1%. Electroporation was transseptal in two hearts. There was no statistical difference ($P = 0.78$) in the depth of electroporation in the septum between the control (n = 5) and MI (n = 5) groups.

In Figure 4C and Table 1, the regional and overall extent of electroporation in MI hearts are summarized. When no shock was delivered, there was virtually no PI accumulation in the MI hearts (striped black). With shock delivery (solid black), the most substantial increase ($P < 0.05$) was found in the shock electrode region ($P < 0.05$ vs all remaining regions within the MI group with shock) similarly to the control group with shock. In the MI group with shock, however, there was an increase ($P < 0.05$) in%PI Volume in the epicardial layer of the aLV region. The overall%PI Volume was increased ($P < 0.05$) to 8.6 ± 2.6% in the MI group compared to the MI hearts without shock.

The extent of electroporation in the control (n = 5, gray) and MI (n = 5, black) groups with shock was further compared in Figure 5. Electroporation in the shock electrode region ($P = 0.15$) as well as the overall extent of electroporation ($P = 0.07$) were similar between the control and MI groups with shocks (Fig. 5A). The aLV Epi region was more vulnerable to shock-induced electroporation in the MI hearts (*, $P < 0.05$). Comparisons of raw tissue volume (mm^3) before normalization confirmed that this difference was independent of heart size (Fig. 5B). There was no significant difference ($P = 0.28$) in the total ventricular tissue volume. The overall PI-accumulated tissue volume in the control and MI groups with shock was also similar

NIH-PA Author Manuscript

NIH-PA Author Manuscript

NIH-PA Author Manuscript

($P = 0.17$). There was, however, significantly ($P < 0.05$) increased PI accumulation in the aLV Epi region of the MI group with shock (banded black) compared with the corresponding region of the control group with shock (banded gray, plotted at 1/100 scale).

Finally, to structurally correlate the heightened susceptibility to shock-induced electroporation in the aLV Epi region, fluorescence and histology images from five MI hearts with shock were compared. In Figure 6, a representative histology image of an MI transverse section is shown in the left column. Higher magnification images from the epicardial layer (red box) and the endocardial layer (green box) are shown in the right column along with the fluorescence images. In all MI hearts with shock, PI accumulation was observed only in a thin surviving epicardial layer (red box). The relatively thick surviving endocardial layer (green box), however, was not stained with PI.

Discussion

In this study, three key observations were made: (1) shock-induced electroporation was closely dependent transversely on the location and longitudinally on the dimension of the active region of the shock electrode; (2) upon one strong internal shock delivery from the RV, the surviving epicardial layer of the infarcted region in the anterior LV free wall was more susceptible to shock-induced electroporation; (3) the overall vulnerability to shock, however, was comparable in the control and MI groups.

In both structurally normal and chronically infarcted rabbit hearts, the most extensive electroporation was confined to the area near the shock electrode. This may be due to the strong transmembrane polarization of cardiac tissue induced near the site of a strong electrical field gradient.[3] This finding can be further evidenced from the apex-to-base spatial dependence of electroporation with respect to the length of the active region of the shock electrode. The spatial distribution of electroporation correlated well with the position and dimension of the shock electrode. The occurrence of electroporation was confirmed to be a shock-induced event, as there was virtually no accumulation of PI within tissue when no shock was delivered in the equivalent experimental setup.

In MI hearts ($n = 5$), electroporation in the aLV Epi region was significantly increased ($P < 0.05$) compared with the corresponding region in control hearts ($n = 5$). Passive diffusion of PI into the surviving anterior epicardial layer alone could not explain this finding because little PI accumulation occurred in this region of MI hearts when no shock was delivered ($P < 0.05$). This suggests that membrane rupture of the surviving epicardial layer may be more easily inducible by the shock application. However, the MI-induced pathophysiologic conditions of the cells occupying the epicardial layer of the infarct appear not to be the sole cause of this increased vulnerability to electroporation because the surviving cells in the relatively thick endocardial layer of aLV were not electroporated. The thickness of the surviving layer may also play a role in the heightened electroporation in the aLV Epi region. However, the mechanism underlying this difference is unclear and further studies are required to elucidate this difference. Al-Khadra *et al.*[3] reported that the endocardium was more susceptible to electroporation. However, it is difficult to correlate the two studies because an internal shock was delivered in the intact heart in this study as opposed to an external shock applied to a dissected tissue preparation in the earlier report. The myocardial structure and electrophysiology of the MI hearts in this study are also different from those of the normal heart used in the study by Al-Khadra *et al.*

The extent of electroporation was substantially larger in the shock electrode region than in the aLV Epi region. Thus, despite significantly increased electroporation in the aLV Epi region of MI hearts, the difference in the overall extent of electroporation between the control and MI

NIH-PA Author Manuscript

NIH-PA Author Manuscript

NIH-PA Author Manuscript

groups did not reach a statistical significance. It was observed during fluorescence imaging that the infarcted region in MI hearts was visually less autofluorescent than the non-infarcted region. The average total ventricular myocardium volume in MI hearts (3,044 ± 502 mm^3; n = 7) tended to be smaller (P = 0.08) than in control hearts (3,650 ± 674 mm^3; n = 7) in fluorescence images. It was not, however, solely due to loss of myocardium to infarction. In histology, the average total ventricular myocardium volume in the control (4,054 ± 628 mm^3; n = 7) and MI (3,825 ± 573 mm^3; n = 7) groups was more comparable (P = 0.49). Following normalization by the histological total tissue volume in the control (n = 5) and MI (n = 5) groups with shock, the statistical comparison of the overall extent of electroporation resulted in P = 0.12. The extent of electroporation remained significantly larger (P < 0.05) in the aLV Epi region of the MI hearts with shock.

PI is a small molecule (668.4 Da) that can theoretically diffuse through gap junction and has been experimentally observed to do so through cardiac connexins, including connexin 43, which is the most abundant connexin in ventricles.[40,41] However, the transfer of PI through connexin 43 gap junctions is limited compared to other dyes such as Lucifer Yellow.[40] This, in conjunction with PI being an intercalating dye that rapidly binds to nucleic acids, greatly limits the ability of PI to diffuse through gap junctions. So, the impact of diffusion on the quantification of the electroporated tissue area would be negligible, even in the thin epicardial layer of the anterior LV free wall of infarcted hearts.

In this study, +300-V shocks were chosen to facilitate the characterization of electroporation. Clinically, ICD shock intensities are determined based on the defibrillation threshold (DFT) of the patient, usually being set at approximately 50–100% above the DFT to obtain an adequate defibrillation safety margin. Although DFT data for the animal model and electrode configuration used in this study are not available, extensive studies have consistently demonstrated that the upper limit of vulnerability (ULV) closely correlates with the DFT.[42] So, the ULV can be used as a surrogate for the DFT in determining rescue shock intensities. In a previous study using the same model and electrode configuration as this study, we found that the average ULV for MI hearts was around +160-V (between +145 V and +175 V, n = 8). Therefore, it is estimated that the clinically equivalent defibrillation shock would be in the range of +240-V to +320-V. Thus, although the shock intensity used in our study was near the higher end, it was still within the clinically relevant range.

Study Limitations

In this study, a single +300 V, 8 ms truncated exponential monophasic shock was delivered in the paced heart. In order to address the limitations of this study and further characterize electroporation in the intact heart, in the future we plan to investigate (1) shock-intensity and polarity-dependent, (2) shock-number and frequency-dependent, and (3) shock-waveform-dependent distribution and extent of electroporation. In addition, delivery of defibrillation shocks in the fibrillating heart would characterize electroporation during more clinically resembling defibrillation. A computer simulation would further enable correlation of experimentally quantified spatial distribution and extent of electroporation to the electrical field gradient within the intact heart model. In this study, electroporation in the infarct region may have been underestimated compared with clinical events because the infarct was mainly in the LV free wall while transseptal MI is often observed in human patients.

Conclusion

In this study, shock-induced electroporation was characterized for the first time in the intact, structurally normal and chronically infarcted hearts. We found electroporation was spatially dependent on the location and dimension of the active region of the shock lead. Electroporation

NIH-PA Author Manuscript

NIH-PA Author Manuscript

NIH-PA Author Manuscript

was more pronounced in the surviving anterior epicardial layer of the infarcted region in MI hearts, which may play an important role in defibrillation.

Supporting Information

The following supporting information is available for this article:

Movie 1. An interactive movie of the three-dimensionally illustrated control heart with shock. The transverse sections shown in the top panel of Figure 2 and in the bottom panel of Figure 3A were pseudocolored and stacked along the long axis. Blue indicates fibrous tissue; green, ventricular myocardium; red, PI fluorescence. Grab and drag the heart with the mouse cursor.

Movie 2. An interactive movie of the three-dimensionally illustrated MI heart with shock. Refer to Movie 1 legend for descriptions. Raw histology and fluorescence images of the transverse sections are shown in the bottom panel of Figure 2 and in the bottom panel of Figure 4A, respectively.

The following Supporting Information is available in the online version of this article.

Please note: Wiley-Blackwell Publishing is not responsible for the content or functionality of any supporting information supplied by the authors. Any queries (other than missing material) should be directed to the corresponding author for the article.

Supplementary Material

Refer to Web version on PubMed Central for supplementary material.

Acknowledgments

The authors thank Mei-Ling Chang Liao and Yves Wang for their excellent technical assistance and Dr. David Van Wagoner for his review of the article.

This study was supported by the National Institutes of Health (Dr. Efimov; R01 HL074283) and the American Heart Association (Dr. Cheng; 0235172N and 0655154B).

References

1. Xie J, Weil MH, Sun S, Tang W, Sato Y, Jin X, Bisera J. High-energy defibrillation increases the severity of postresuscitation myocardial dysfunction. Circulation 1997;96:683–688. [PubMed: 9244243]
2. Sambelashvili AT, Nikolski VP, Efimov IR. Virtual electrode theory explains pacing threshold increase caused by cardiac tissue damage. Am J Physiol Heart Circ Physiol 2004;286:H2183–H2194. [PubMed: 14726298]
3. Al-Khadra AS, Nikolski V, Efimov IR. The role of electroporation in defibrillation. Circ Res 2000;87:797–804. [PubMed: 11055984]
4. Li L, Nikolski V, Wallick DW, Efimov IR, Cheng Y. Mechanisms of enhanced shock-induced arrhythmogenesis in the rabbit heart with healed myocardial infarction. Am J Physiol Heart Circ Physiol 2005;289:H1054–H1068. [PubMed: 15879480]
5. Lee RC. Injury by electrical forces: Pathophysiology, manifestations, and therapy. Curr Probl Surg 1997;34:677–764. [PubMed: 9365421]
6. Harrison RL, Byrne BJ, Tung L. Electroporation-mediated gene transfer in cardiac tissue. FEBS Lett 1998;435:1–5. [PubMed: 9755847]
7. Trollet C, Bloquel C, Scherman D, Bigey P. Electrotransfer into skeletal muscle for protein expression. Curr Gene Ther 2006;6:561–578. [PubMed: 17073602]

NIH-PA Author Manuscript

NIH-PA Author Manuscript

NIH-PA Author Manuscript

8. Weaver JC. Electroporation: A general phenomenon for manipulating cells and tissues. J Cell Biochem 1993;51:426–435. [PubMed: 8496245]
9. Jones JL, Jones RE, Balasky G. Microlesion formation in myocardial cells by high-intensity electric field stimulation. Am J Physiol 1987;253:H480–H486. [PubMed: 2441612]
10. Cheng DK, Tung L, Sobie EA. Nonuniform responses of transmembrane potential during electric field stimulation of single cardiac cells. Am J Physiol 1999;277:H351–H362. [PubMed: 10409215]
11. Knisley SB, Grant AO. Asymmetrical electrically induced injury of rabbit ventricular myocytes. J Molecular Cell Cardiol 1995;27:1111–1122.
12. Tovar O, Tung L. Electroporation and recovery of cardiac cell membrane with rectangular voltage pulses. Am J Physiol 1992;263(Pt 2):H1128–1136. [PubMed: 1415761]
13. Cheek ER, Fast VG. Nonlinear changes of transmembrane potential during electrical shocks: role of membrane electroporation. Circ Res 2004;94:208–214. [PubMed: 14670844]
14. Neunlist M, Tung L. Dose-dependent reduction of cardiac transmembrane potential by high-intensity electrical shocks. Am J Physiol 1997;273:H2817–H2825. [PubMed: 9435619]
15. Aguel F, DeBruin KA, Krassowska W, Trayanova NA. Effects of electroporation on the transmembrane potential distribution in a two-dimensional bidomain model of cardiac tissue. J Cardiovasc Electrophysiol 1999;10:701–714. [PubMed: 10355926]
16. DeBruin KA, Krassowska W. Electroporation and shock-induced transmembrane potential in a cardiac fiber during defibrillation strength shocks. Ann Biomed Eng 1998;26:584–596. [PubMed: 9662151]
17. Krauthamer V, Jones JL. Calcium dynamics in cultured heart cells exposed to defibrillator-type electric shocks. Life Sci 1997;60:1977–1985. [PubMed: 9180351]
18. Kodama I, Shibata N, Sakuma I, Mitsui K, Iida M, Suzuki R, Fukui Y, Hosoda S, Toyama J. Aftereffects of high-intensity DC stimulation on the electromechanical performance of ventricular muscle. Am J Physiol 1994;267:H248–H258. [PubMed: 7519406]
19. Nikolski VP, Efimov IR. Electroporation of the heart. Europace 2005;7:S146–S154.
20. Janks DL, Roth BJ. Simulations of optical mapping during electroporation. Conf Proc IEEE Eng Med Biol Soc 2004;5:3581–3584. [PubMed: 17271065]
21. Ashihara T, Trayanova NA. Cell and tissue responses to electric shocks. Europace 2005;7(Suppl 2): 155–165. [PubMed: 16102513]
22. Ashihara T, Yao T, Namba T, Ito M, Ikeda T, Kawase A, Toda S, Suzuki T, Inagaki M, Sugimachi M, Kinoshita M, Nakazawa K. Electroporation in a model of cardiac defibrillation. J Cardiovasc Electrophysiol 2001;12:1393–1403. [PubMed: 11797997]
23. Ohuchi K, Fukui Y, Sakuma I, Shibata N, Honjo H, Kodama I. A dynamic action potential model analysis of shock-induced aftereffects in ventricular muscle by reversible breakdown of cell membrane. IEEE Trans Biomed Eng 2002;49:18–30. [PubMed: 11794768]
24. Efimov IR, Gray RA, Roth BJ. Virtual electrodes and de-excitation: New insights into fibrillation induction and defibrillation. J Cardiovasc Electrophysiol 2000;11:339–353. [PubMed: 10749359]
25. Efimov IR, Cheng Y, Yamanouchi Y, Tchou PJ. Direct evidence of the role of virtual electrode induced phase singularity in success and failure of defibrillation. J Cardiovasc Electrophysiol 2000;11:861–868. [PubMed: 10969748]
26. Efimov IR, Cheng Y, Van Wagoner DR, Mazgalev T, Tchou PJ. Virtual electrode-induced phase singularity: A basic mechanism of failure to defibrillate. Circ Res 1998;82:918–925. [PubMed: 9576111]
27. Krassowska W. Effects of electroporation on transmembrane potential induced by defibrillation shocks. Pacing Clin Electrophysiol 1995;18:1644–1660. [PubMed: 7491308]
28. Janse MJ, Wit AL. Electrophysiological mechanisms of ventricular arrhythmias resulting from myocardial ischemia and infarction. Physiol Rev 1989;69:1049–1169. [PubMed: 2678165]
29. Downar E, Saito J, Doig JC, Chen TC, Sevaptsidis E, Masse S, Kimber S, Mickleborough L, Harris L. Endocardial mapping of ventricular tachycardia in the intact human ventricle. III. Evidence of multiuse reentry with spontaneous and induced block in portions of reentrant path complex. J Am Coll Cardiol 1995;25:1591–1600. [PubMed: 7759710]

NIH-PA Author Manuscript

NIH-PA Author Manuscript

NIH-PA Author Manuscript

30. Misier AR, Opthof T, van Hemel NM, Vermeulen JT, de Bakker JM, Defauw JJ, van Capelle FJ, Janse MJ. Dispersion of 'refractoriness' in noninfarcted myocardium of patients with ventricular tachycardia or ventricular fibrillation after myocardial infarction. Circulation 1995;91:2566–2572. [PubMed: 7743618]

31. Nikolski VP, Sambelashvili AT, Krinsky VI, Efimov IR. Effects of electroporation on optically recorded transmembrane potential responses to high-intensity electrical shocks. Am J Physiol Heart Circ Physiol 2004;286:H412–H418. [PubMed: 14527941]

32. Tsong TY. Electroporation of cell membranes. Biophys J 1991;60:297–306. [PubMed: 1912274]

33. Lavee J, Onik G, Mikus P, Rubinsky B. A novel nonthermal energy source for surgical epicardial atrial ablation: Irreversible electroporation. Heart Surg Forum 2007;10:E162–E167. [PubMed: 17597044]

34. Ootaki Y, Yamada H, Daimon M, Kamohara K, Popovic Z, Van Wagoner DR, Cheng Y, Fukamachi K. An experimental rabbit model for off-pump left ventricular reconstruction following left ventricular aneurysm. Heart Surg Forum 2006;9:E786–E791. [PubMed: 17099973]

35. Podesser B, Wollenek G, Seitelberger R, Siegel H, Wolner E, Firbas W, Tschabitscher M. Epicardial branches of the coronary arteries and their distribution in the rabbit heart: The rabbit heart as a model of regional ischemia. Anat Rec 1997;247:521–527. [PubMed: 9096792]

36. Lee BH, Kim WH, Choi MJ, Rho JR, Kim WG. Chronic heart failure model in rabbits based on the concept of the bifurcation/trifurcation coronary artery branching pattern. Artificial Organs 2002;26:360–365. [PubMed: 11952507]

37. Efimov IR, Cheng YN, Biermann M, Van Wagoner DR, Mazgalev T, Tchou PJ. Transmembrane voltage changes produced by real and virtual electrodes during monophasic defibrillation shock delivered by an implantable electrode. J Cardiovasc Electrophysiol 1997;8:1031–1045. [PubMed: 9300301]

38. Cheng Y, Mowrey KA, Nikolski V, Tchou PJ, Efimov IR. Mechanisms of shock-induced arrhythmogenesis during acute global ischemia. Am J Physiol 2002;282:H2141–H2151.

39. Takagawa J, Zhang Y, Wong ML, Sievers RE, Kapasi NK, Wang Y, Yeghiazarians Y, Lee RJ, Grossman W, Springer ML. Myocardial infarct size measurement in the mouse chronic infarction model: Comparison of area- and length-based approaches. J Appl Physiol 2007;102:2104–2111. [PubMed: 17347379]

40. Elfgang C, Eckert R, Lichtenberg-Frate H, Butterweck A, Traub O, Klein RA, Hulser DF, Willecke K. Specific permeability and selective formation of gap junction channels in connexin-transfected HeLa cells. J Cell Biol 1995;129:805–817. [PubMed: 7537274]

41. Rackauskas M, Verselis VK, Bukauskas FF. Permeability of homotypic and heterotypic gap junction channels formed of cardiac connexins mCx30.2, Cx40, Cx43, and Cx45. Am J Physiol Heart Circ Physiol 2007;293:H1729–H1736. [PubMed: 17557922]

42. Swerdlow CD, Shehata M, Chen PS. Using the upper limit of vulnerability to assess defibrillation efficacy at implantation of ICDs. Pacing Clin Electrophysiol 2007;30:258–270. [PubMed: 17338725]

NIH-PA Author Manuscript
NIH-PA Author Manuscript
NIH-PA Author Manuscript

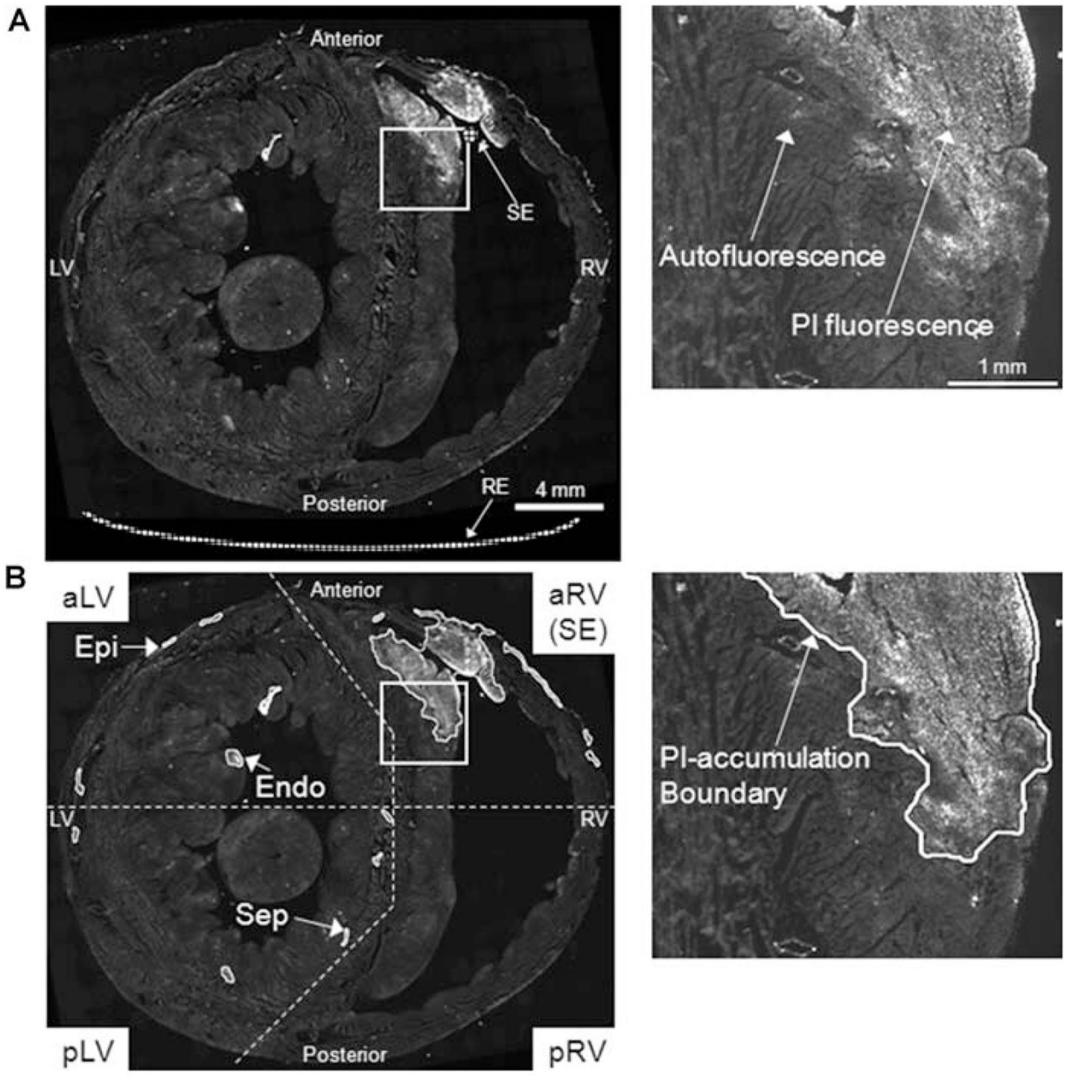

Figure 1.

PI-staining of nuclei upon shock delivery. PI-stained nuclei appear as bright fluorescence signal while tissue autofluorescence is also visible. The right column shows a magnified view of the white box in the left column image. (A) A raw mosaic image of the entire ventricular transverse section. The shock electrode (SE) and reference electrode (RE) positions are schematically illustrated. (B) The transverse section shown in A was processed for PI quantification. Clusters of PI-accumulated tissue were identified, and PI-accumulation boundaries were traced. The transverse sections were divided into four regions as shown in the left column. Each region except the SE region was further categorized into three subregions according to tissue structure. PI-accumulations in the epicardial (Epi) and endocardial (Endo) layers of the anterior and anterolateral LV region (aLV), and in the septal region (Sep) of the posterior and posterolateral LV region (pLV) were exemplarily indicated. (Same scales as in A; aRV = anterior and anterolateral RV; pRV = posterior and posterolateral RV; aLV = anterior and anterolateral LV; pLV = posterior and posterolateral LV; Epi = epicardial layer of the free wall; Endo = endocardial layer of the free wall; Sep = septum.)

NIH-PA Author Manuscript

NIH-PA Author Manuscript

NIH-PA Author Manuscript

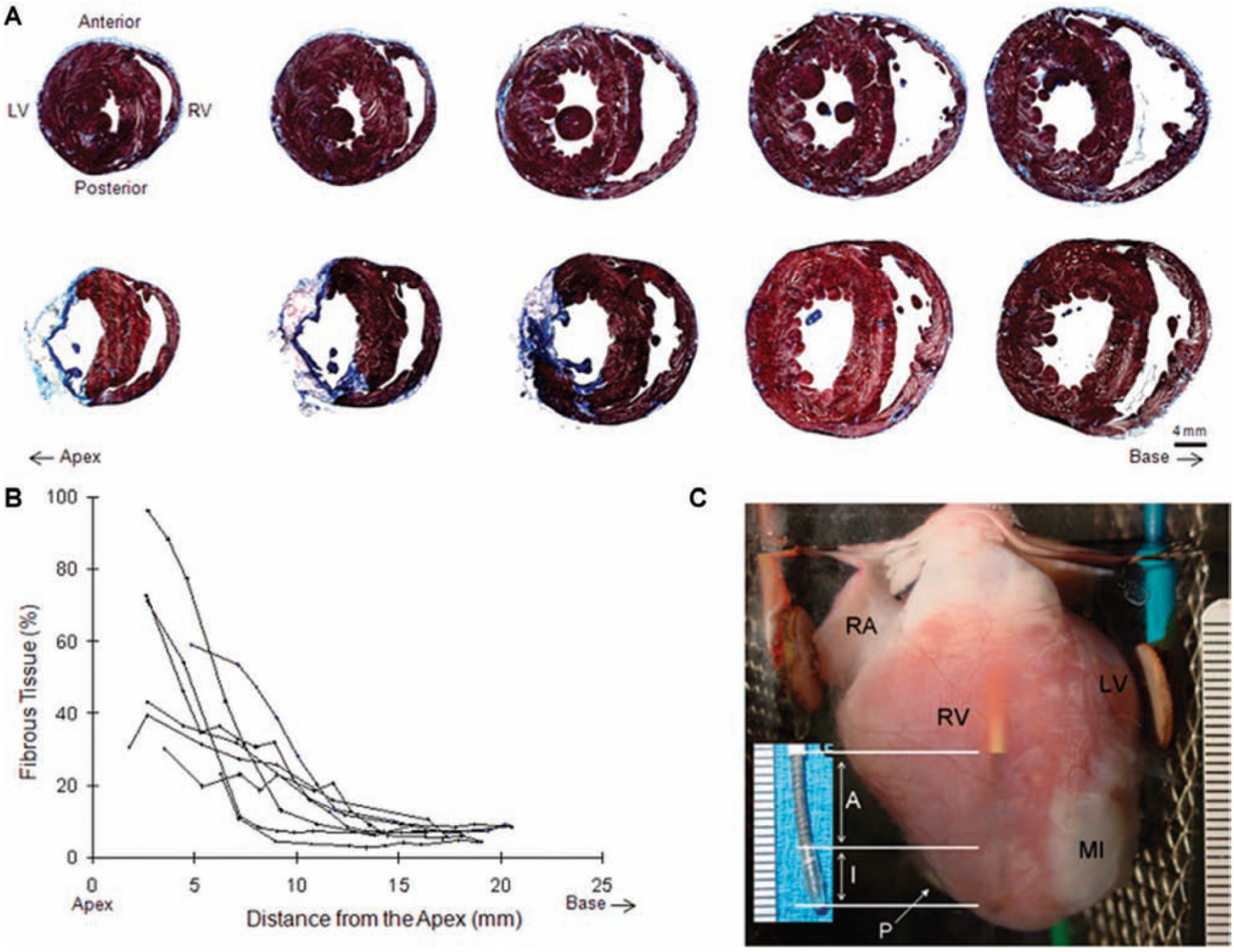

Figure 2.

Histology. (A) Transverse sections from the control (top panel) and MI (bottom panel) groups were stained by Masson's trichrome. Muscle was stained in red while fibrous scar tissue was stained in blue. The series of sections are shown from the apex (left) toward the base (right). Fluorescence images of the same transverse sections are shown in the bottom panels of Figures 3A and 4A, respectively. (B) Fibrous tissue content was quantified along the long axis of MI hearts (n = 8). MI scar was mostly confined in the apex. (C) An MI heart preparation. The shock electrode (SE) inserted in RV is visible through the anterior RV free wall. The distal tip of the shock electrode (inset) was composed of a 6 mm nonconducting inactive region (I) and a 10 mm active region (A). The pacing electrode (P) was positioned at the apex of the posterior RV free wall (RA = right atrium).

NIH-PA Author Manuscript

NIH-PA Author Manuscript

NIH-PA Author Manuscript

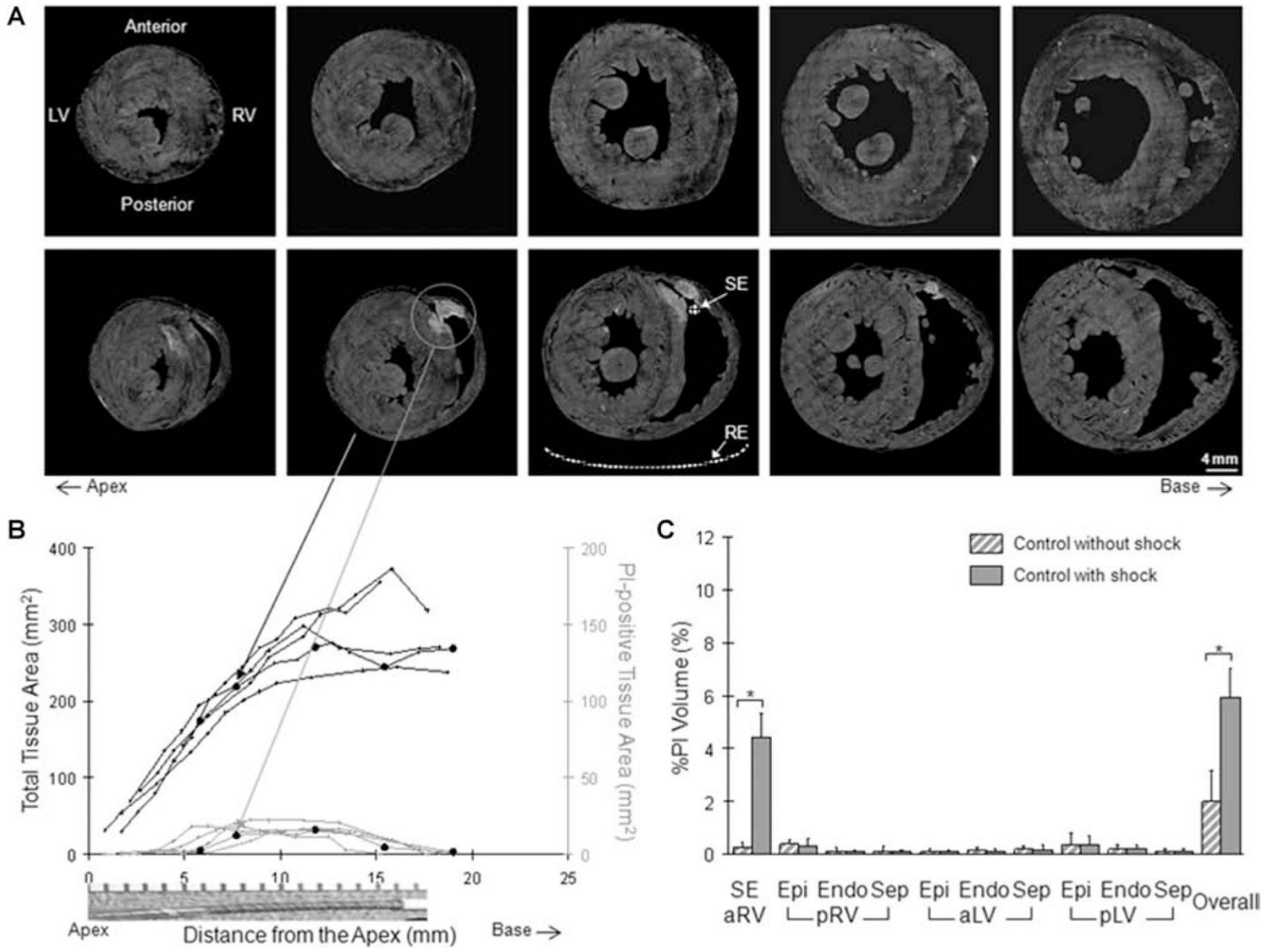

Figure 3.

Fluorescence study of the control group. (A) Series of transverse sections from the control hearts without shock (top row) and with shock (bottom row). The shock electrode (SE) and reference electrode (RE) positions are representatively illustrated. (B) Electroporation was quantified in the shock electrode region along the long axis of the heart. The circle markers represent measurements from the transverse sections shown in the bottom row of A. A picture of the shock electrode is shown for spatial correspondence. (C) The regional and overall extent of electroporation in the control group with and without shock was integrated along the long axis of the heart. *$P < 0.05$.

NIH-PA Author Manuscript

NIH-PA Author Manuscript

NIH-PA Author Manuscript

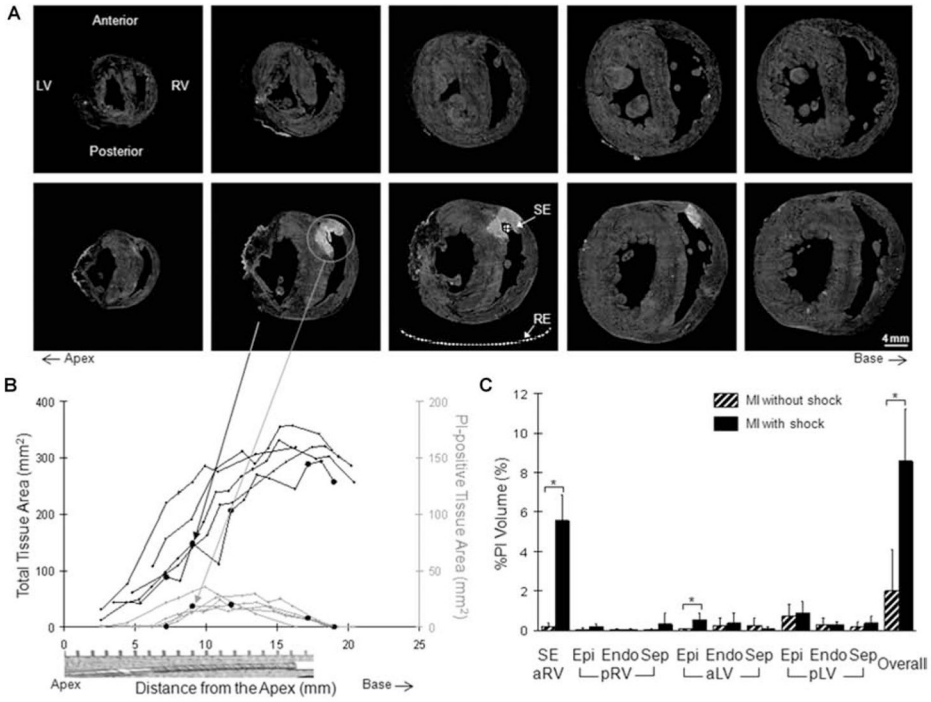

Figure 4.
Fluorescence study of the MI group. Refer to Figure 3 legend for descriptions.

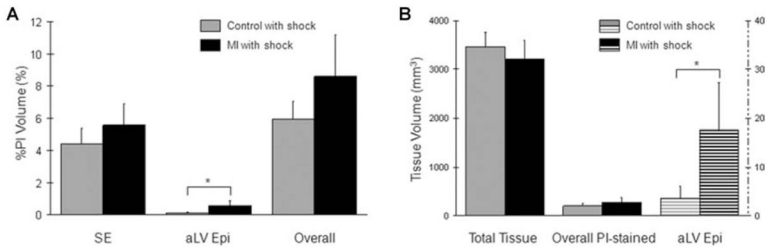

Figure 5.

Comparison of the extent of electroporation. (A) The regional and overall extent of electroporation is compared between the control and MI groups with shock. (B) Raw measurements of the total tissue volume (Total Tissue) and the PI-accumulated tissue volume in the entire ventricles (Overall PI-stained) as well as in the aLV Epi region (plotted at 1/100 scale) are compared between the control and MI groups with shock. (*, $P < 0.05$)

NIH-PA Author Manuscript
NIH-PA Author Manuscript
NIH-PA Author Manuscript

NIH-PA Author Manuscript

NIH-PA Author Manuscript

NIH-PA Author Manuscript

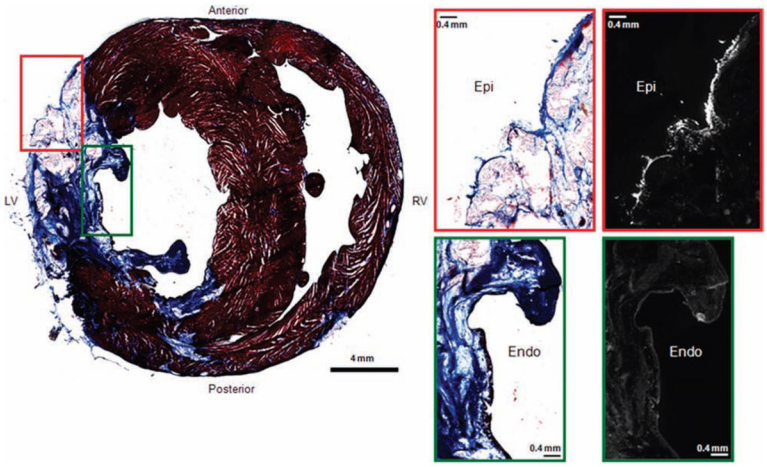

Figure 6.
Correlation of histology and fluorescence study. A histology image of an MI transverse section is shown in the left column. Higher magnification images from the epicardial layer (red box) and the endocardial layer (green box) are shown in the right column along with the fluorescence images.

NIH-PA Author Manuscript
NIH-PA Author Manuscript
NIH-PA Author Manuscript

TABLE 1

Regional and Overall Electroporation

%PI Volume (%)		Control (N = 8)		MI (N = 8)	
		Without Shock (N = 3)	With Shock (N = 5)	Without Shock (N = 3)	With Shock (N = 5)
Regional					
ARV	SE	0.32 ± 0.22	4.42 ± 0.93*	0.20 ± 0.18	5.55 ± 1.30*
PRV	Epi	0.50 ± 0.08	0.29 ± 0.34	0.04 ± 0.07	0.18 ± 0.16
	Endo	0.16 ± 0.16	0.10 ± 0.06	0.04 ± 0.05	0.04 ± 0.03
	Sep	0.17 ± 0.21	0.08 ± 0.08	0.04 ± 0.06	0.30 ± 0.55
ALV	Epi	0.14 ± 0.05	0.10 ± 0.07	0.05 ± 0.05	0.55 ± 0.32*,†
	Endo	0.18 ± 0.11	0.11 ± 0.09	0.25 ± 0.39	0.36 ± 0.49
	Sep	0.15 ± 0.13	0.16 ± 0.18	0.24 ± 0.41	0.10 ± 0.09
PLV	Epi	0.53 ± 0.43	0.35 ± 0.35	0.72 ± 0.62	0.88 ± 0.57
	Endo	0.28 ± 0.05	0.20 ± 0.18	0.27 ± 0.33	0.28 ± 0.17
	Sep	0.13 ± 0.11	0.11 ± 0.12	0.16 ± 0.24	0.36 ± 0.34
Overall		2.55 ± 0.92	5.93 ± 1.12*	2.01 ± 2.07	8.60 ± 2.60**

*$P < 0.05$, versus same group without shock;

†versus control group with shock. MI = myocardial infarction; aRV = the anterior and anterolateral RV free wall and approximately one-fourth of the septum that is in a close vicinity to the shock electrode (SE); pRV = posterior and posterolateral RV free wall and the adjacent septum; aLV = the anterior and anterolateral LV free wall and the adjacent septum; pLV = the posterior and posterolateral LV free wall and the adjacent septum (pLV). Epi = the epicardial layer defined as a portion of the free wall from the epicardium to the mid-wall. Endo = endocardial layer consists of the remaining free wall inclusive of the endocardium. Sep = the septal region includes a portion of the septum within each respective region.